IJIE

INTERNATIONAL JOURNAL OF INTEGRATED ENGINEERING
ISSN: 2229-838X e-ISSN: 2600-7916

Vol. 18 No. 2 (2026) 269-277
https://publisher.uthm.edu.my/ojs/index.php/ijie

# PVA-Assisted Sol-Gel Synthesis and Structural Characterisation of CuO-Coated $LiMnPO_4$ Olivines

**K. Rajammal[1], D. Sivakumar[2]*, M. Z. Selamat[2], R. Nadlene[2], C. K. Kok[3]**

[1] *Centre for Foundation and General Studies, Manipal University College Malaysia, 75150 Bukit Baru, Melaka, MALAYSIA*
[2] *Fakulti Teknologi dan Kejuruteraan Mekanikal, Universiti Teknikal Malaysia Melaka, 76100 Durian Tunggal, Melaka, MALAYSIA*
[3] *Centre for Advanced Mechanical and Green Technology, Faculty of Engineering and Technology, Multimedia University, 75450 Bukit Beruang, Melaka, MALAYSIA*

*Corresponding Author: sivakumard@utem.edu.my
DOI: https://doi.org/10.30880/ijie.2026.18.02.021

**Article Info**

Received: 3 November 2025
Accepted: 15 March 2026
Available online: 18 May 2026

**Keywords**

$LiMnPO_4$, sol-gel method, cathode materials, electrochemical properties, lithium-ion batteries

**Abstract**

This study examines the influence of different weight percentages of CuO coating (1, 2, and 3 wt.%) on the structural properties of $LiMnPO_4$ cathode materials synthesised by the polyvinyl alcohol (PVA)-assisted sol–gel method. PVA acted as a carbon source during synthesis, producing an in situ carbon layer that improves the conductivity of the composite. XRD analysis confirmed the formation of a pure olivine $LiMnPO_4$ phase without impurity peaks, indicating that the CuO coating did not alter the main structure. SEM and EDAX analyses verified the uniform distribution of the CuO layer and the presence of carbon. The 2 wt.% CuO-coated sample showed the smallest crystallite size (33.8 nm) and the lowest strain value ($1.28 \times 10^{-3}$), compared to the pristine $LiMnPO_4$ (86.6 nm, $2.43 \times 10^{-3}$). These results suggest that the optimised CuO coating helps control particle growth and enhances structural uniformity, which could contribute to better electrochemical stability in future applications.

## 1. Introduction

Lithium-ion batteries (LIBs) remain the dominant energy-storage technology for portable electronic devices and hybrid electric vehicles because of their high energy density, long cycle life, and efficiency [1]. Continuous improvements in LIB performance rely strongly on the development of advanced electrode materials that exhibit better structural stability, thermal safety, and electronic properties compared to conventional ones. Olivine phosphate cathodes are among the most studied polyanion materials because their strong P–O bonds provide excellent structural stability and safety during cycling [2, 3].

Within this class, $LiMnPO_4$ has been identified as one of the most promising cathode materials because it offers a higher operating voltage (~4.1 V vs. $Li^+/Li$) and greater theoretical energy density than $LiFePO_4$ [4–6]. $LiMnPO_4$ crystallises in an orthorhombic olivine structure (space group Pnma), where $Mn^{2+}$ ions occupy octahedral sites linked through $PO_4$ tetrahedra, forming one-dimensional lithium diffusion channels along the b-axis. Despite these advantages, $LiMnPO_4$ suffers from very low intrinsic electronic conductivity (~$10^{-9}$ S $cm^{-1}$) and limited lithium-ion mobility, both of which hinder its practical performance [7]. Furthermore, the Jahn–Teller distortion associated with high-spin $Mn^{3+}$ ions can destabilise the lattice and degrade structural uniformity during synthesis or cycling [8, 9].

Efforts to overcome these limitations have included cation substitution, particle downsizing, carbon coating, and surface modification with various metal oxides [8, 10–17]. Among these strategies, metal-oxide coating has proven particularly effective, as it can mitigate unwanted side reactions, reduce surface defects, and improve both structural and interfacial stability. Thin oxide layers such as $Al_2O_3$ and ZnO have been reported to act as protective barriers that preserve the olivine framework and inhibit Mn dissolution [18–20]. Nevertheless, there has been relatively little systematic investigation into the structural effects of CuO surface coatings on $LiMnPO_4$, especially regarding their influence on crystallite refinement, lattice strain, and microstructural evolution. Most prior studies emphasise electrochemical behaviour, providing only limited structural analysis.

Polymer-assisted sol–gel synthesis has emerged as a versatile approach for producing fine, compositionally homogeneous powders with controlled morphology [21]. In this context, polyvinyl alcohol (PVA) serves as an efficient chelating and binding agent that promotes uniform metal-ion dispersion during the gelation process. Upon calcination, PVA decomposes to form residual carbon, which can enhance electrical connectivity and limit particle growth [22–26]. The incorporation of CuO coating into a PVA-assisted sol–gel process offers a dual advantage: (i) CuO can stabilise the $LiMnPO_4$ structure through surface modification, and (ii) the in situ carbon formation helps prevent agglomeration while slightly improving conductivity[27]. This combined approach provides a promising route to produce structurally robust and uniformly coated olivine-type $LiMnPO_4$ powders.

The present study focuses on the synthesis and structural characterisation of CuO-coated $LiMnPO_4$ olivines prepared by a PVA-assisted sol–gel method. The work aims to elucidate how varying CuO concentrations (1–3 wt%) affect crystallite size, lattice strain, and phase stability. Structural parameters were determined from X-ray diffraction data using Williamson–Hall analysis, while surface morphology and elemental distribution were examined via field-emission scanning electron microscopy and energy-dispersive X-ray spectroscopy. Fourier-transform infrared spectroscopy was used to confirm the preservation of the phosphate framework and bonding environment. By correlating CuO coating content with microstructural features, this study provides new insights into the structural evolution of $LiMnPO_4$ olivines and clarifies how CuO surface engineering contributes to lattice stability. The findings are expected to assist in the rational design of structurally optimised olivine phosphates for advanced functional applications.

## 2. Materials and Methods

### 2.1 Synthesis of $LiMnPO_4$

$LiMnPO_4$ powder was synthesised via a PVA-assisted sol–gel method via similar sol-gel method described elsewhere [28]. Analytical grade reagents were used without further purification: lithium acetate dihydrate ($LiC_2H_3O_2$) (Aldrich), manganese acetate tetrahydrate $Mn(CH_3COO)_2{\cdot}4H_2O$ (Friendmann Schmidt), and ammonium dihydrogen phosphate $(NH_4)H_2PO_4$ (Friendmann Schmidt). Stoichiometric amounts of 0.02 mol for each precursor were dissolved in 100 mL of distilled water under constant magnetic stirring at 80 °C. A few drops of nitric acid (10 mL, 1 M) were added to ensure complete dissolution of the salts. Subsequently, 2 wt.% of polyvinyl alcohol (PVA)(Sigma-Aldrich) with respect to the total solute mass was introduced as a polymeric binder and carbon precursor. The mixture was continuously stirred and heated until dry gelation occurred. The resulting xerogel was ground into fine powder and sintered at 700 °C for 3 h in an air atmosphere to obtain phase-pure $LiMnPO_4$. During calcination, PVA decomposed to yield a thin carbon layer on the $LiMnPO_4$ particles, which enhances electrical connectivity and prevents excessive particle growth.

### 2.2 CuO Coating Procedure

To prepare CuO-coated samples, copper(II) acetate monohydrate ($Cu(CH_3COO)_2{\cdot}H_2O$)(Friendmann Schmidt)was dissolved in 50 mL of ethanol and magnetically stirred at 70 °C until a clear solution was obtained. The as-prepared $LiMnPO_4$ powder was then added to this solution and stirred for 1 h to ensure uniform adsorption of $Cu^{2+}$ ions on the particle surfaces. The solvent was slowly evaporated, yielding a homogeneous precursor powder. Samples containing 1 wt.%, 2 wt.%, and 3 wt.% CuO with respect to $LiMnPO_4$ were prepared and subsequently sintered at 700 °C for 3 h. During heating, the copper precursor decomposed to CuO, forming a uniform surface coating on the $LiMnPO_4$ particles. This coating acts as a conductive interface that enhances electron transport and stabilises the surface against structural degradation. Fig. 1 illustrates the synthesis of $LiMnPO_4$ and the CuO coating process.

Int. Journal of Integrated Engineering Vol. 18 No. 2 (2026) p. 269-277

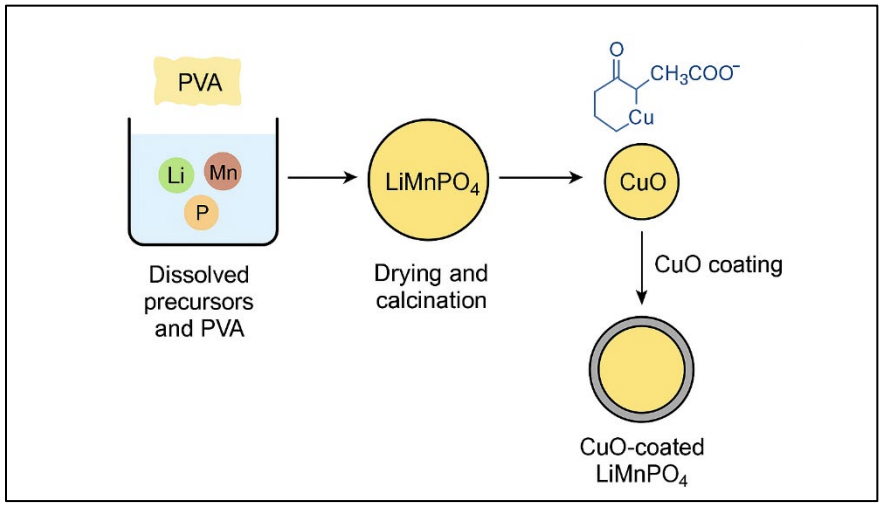


**Fig. 1** *Schematic illustration of the PVA-assisted sol-gel synthesis and CuO coating process for LiMnPO4 olivines*

## 2.3 Characterisation

The crystalline nature of the obtained sample was verified by X-ray diffraction (XRD, Panalytical X'pert Pro brand). The surface texture of the sample and composition mapping were analysed by scanning electron microscope (SEM, JEOL JSM-6010PLUS/LV). FTIR spectra were obtained using Jasco FT/IR-6100 equipment.

## 3. Results and Discussion

The XRD patterns of pristine and CuO-coated $LiMnPO_4$ powders are shown in Fig. 2. All diffraction peaks are indexed to the orthorhombic olivine structure (JCPDS 33-0804), confirming the successful synthesis of phase-pure $LiMnPO_4$ without detectable impurities [12, 29]. The most intense diffraction peak at ~35° corresponds to the (131) plane [30], while additional peaks at 20.4°, 25.1°, and 29.1° are assigned to the (011), (111/021), and (200/121) planes, respectively [12, 29]. The alignment of these peaks with standard 2θ values verifies the complete formation of $LiMnPO_4$.

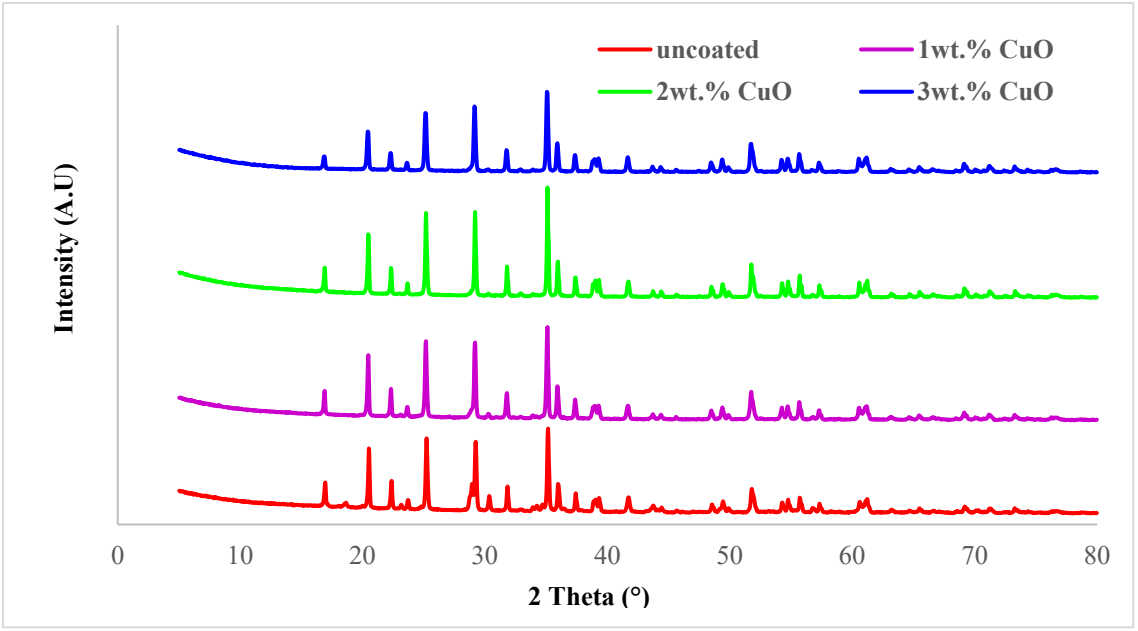


**Fig. 2** *XRD of pristine and CuO coated samples*

The absence of additional CuO peaks even at 3 wt.% coating indicates that CuO did not alter the bulk structure but remained as a thin surface layer. This structural integrity demonstrates that the coating process preserves the original crystal framework while introducing surface modification. Compared with the pristine sample, a slight

peak broadening in coated samples reflects the formation of smaller crystallites, consistent with the Williamson–Hall analysis. However, the presence of a thin CuO layer on $LiMnPO_4$ was validated by EDAX analysis, as in Fig. 3. FESEM images depict smaller particles that are clumped together like a cauliflower shape for a pristine $LiMnPO_4$ sample (Fig. 3a). After CuO coating, the particles appear more distinct and uniformly distributed. The 1 wt.% and 2 wt.% CuO-coated samples show smoother surfaces and reduced agglomeration (Fig. 3b and 3c), while the 3 wt.% sample displays slight irregularity due to excessive coating (Fig. 3d). EDAX spectra confirm the presence of Cu and C elements, verifying successful CuO coating and carbon incorporation from PVA. The coexistence of CuO and carbon likely provides synergistic effects. CuO improves the electronic contact, while carbon minimises grain boundary resistance. This dual contribution is essential for enhancing the overall conductivity and electrochemical performance of the cathode material [31].

The crystallites within the particles were analysed further with the aid of the Williamson-Hall method [32–36]. Based on equation (1).

$$B\cos\theta = \frac{K\lambda}{t} + 4\varepsilon\sin\theta \quad (1)$$

where $B$, $\theta$, $K$, $\lambda$, $t$ and $\varepsilon$ are the full width half maximum (FWHM), Bragg angle, constant value (0.9), wavelength of the radiation (1.54056 Å), mean crystallite size and average strain, respectively. The graph was plotted $\beta \cos \theta$ versus $\sin \theta$ as displayed in Fig. 4. The micro-strain value was calculated based on the gradient and the crystallite size from the intercept value at the vertical axis.

The crystallite sizes and strain values obtained from the graphs are listed in Table 1. It indicates that coated samples with smaller crystallites and strain values compared to the pristine sample. 2wt.% CuO coated sample reveals the smallest mean crystallite size among the samples, followed by 3wt.% CuO coated sample. Nevertheless, the range is between 33.8 nm – 35.5 nm. These results indicate that CuO coating effectively controls particle and crystallite growth. Smaller crystallite size improves $Li^+$ diffusion by shortening the diffusion path and increasing the active surface area, while lower micro strain reflects improved lattice uniformity and fewer defect sites. These structural modifications are favourable for maintaining mechanical stability and minimising volume change during lithium intercalation and deintercalation processes [36].

**Table 1** *Crystallite size and strain values of the samples*

| Samples | Crystallite Size (nm) | Strain ($\times 10^{-3}$) |
|---|---|---|
| Pristine | 86.6 | 2.43 |
| 1wt.% CuO | 53.3 | 2.05 |
| 2wt.% CuO | 33.8 | 1.28 |
| 3wt.% CuO | 35.5 | 1.18 |

FTIR of $LiMnPO_4$ and CuO coated $LiMnPO_4$ samples is given in Fig. 5. FTIR provides information about cation arrangement within the samples. It can be described in terms of four significant modes of vibrations as follows. $\nu_1$ is non-degenerate, $\nu_2$ is doubly degenerate, whereas $\nu_3$ and $\nu_4$ as triply degenerate and infrared active, respectively. $\nu_1$ positioned around 968 $cm^{-1}$, $\nu_2$ located at 470 $cm^{-1}$, $\nu_3$ between1000 $cm^{-1}$ and 1150 $cm^{-1}$ and $\nu_4$ around 530 $cm^{-1}$ and 650 $cm^{-1}$ [37]. The samples denote all these modes of vibrations.

Int. Journal of Integrated Engineering Vol. 18 No. 2 (2026) p. 269-277

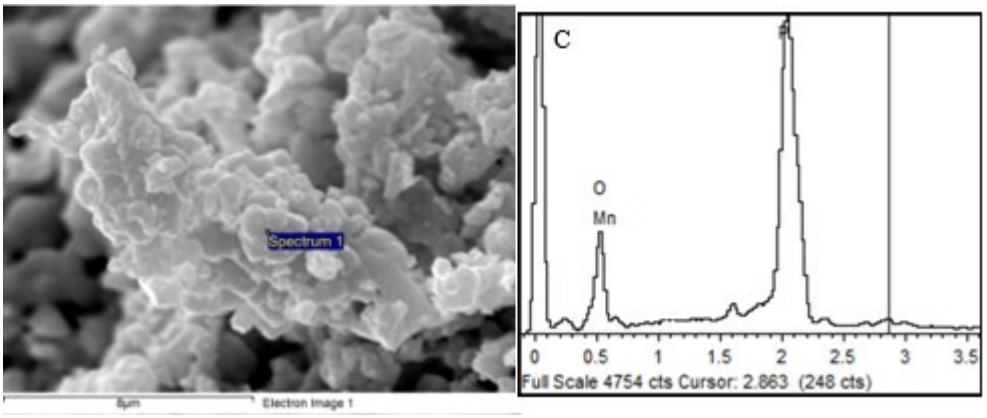


**(a) Pristine**

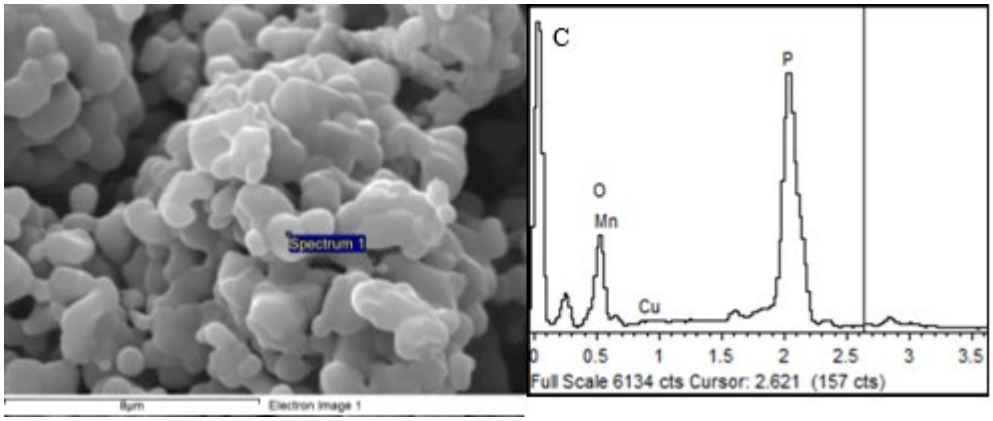


**(b) 1 wt%**

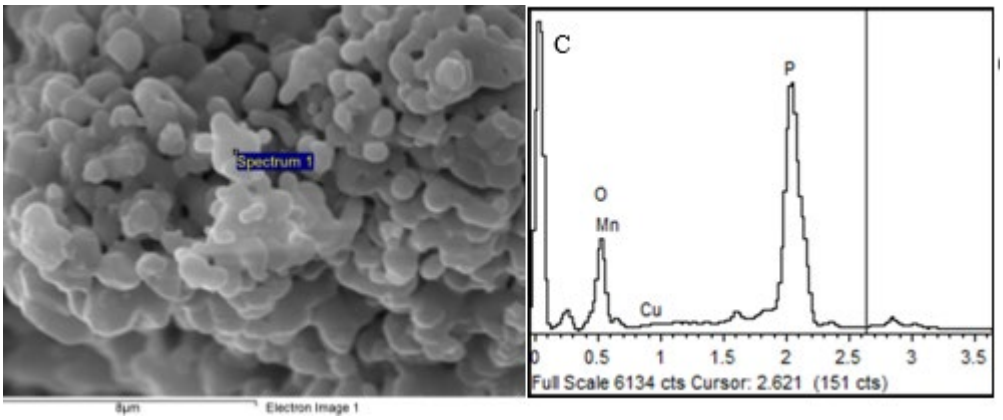


**(c) 2 wt%**

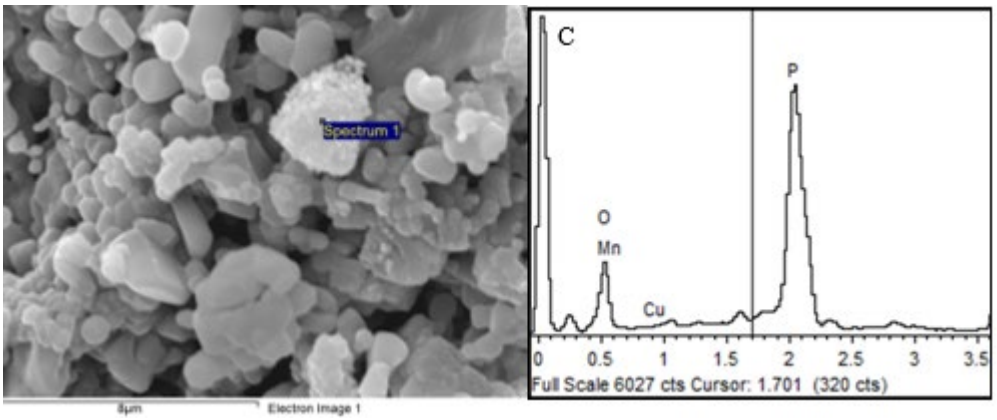


**(d) 3 wt%**

**Fig. 3** *SEM and EDAX of pristine and coated samples*

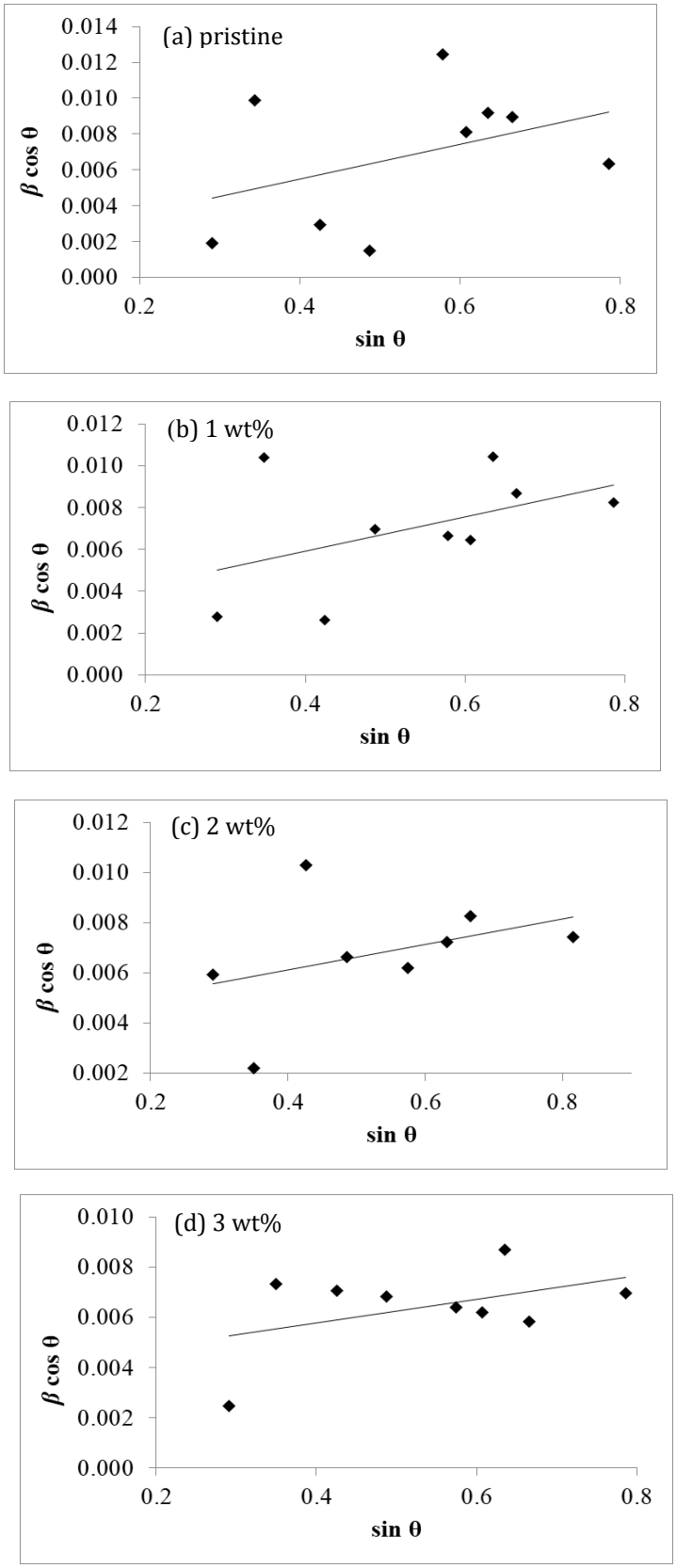


**Fig. 4** *W-H plots of the pristine and CuO coated samples*

Int. Journal of Integrated Engineering Vol. 18 No. 2 (2026) p. 269-277

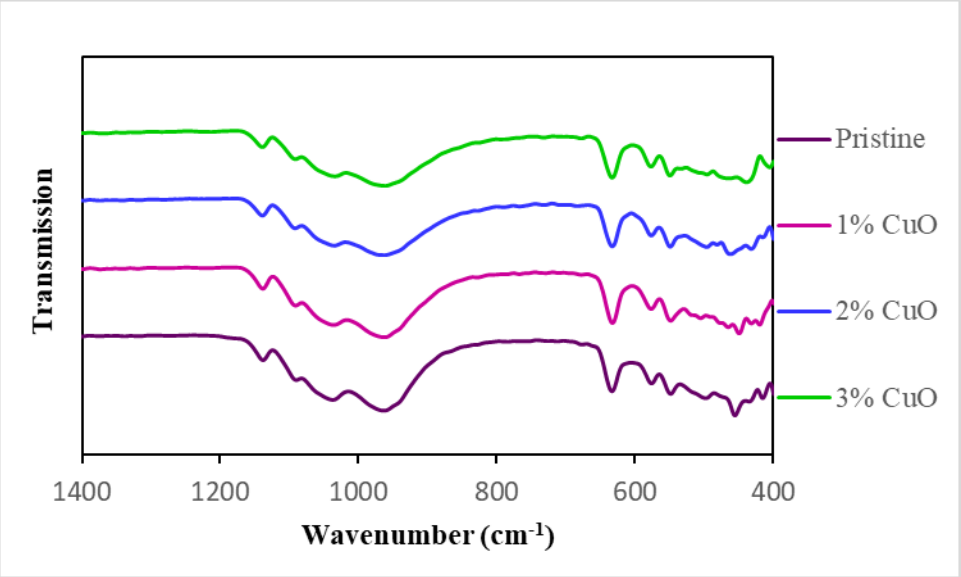


**Fig. 5** *FTIR of pristine and CuO coated samples*

## 4. Conclusion

CuO-coated $LiMnPO_4$ olivines were successfully synthesised via a polyvinyl-alcohol-assisted sol–gel method, and their structural features were systematically investigated as a function of coating content. X-ray diffraction confirmed the formation of single-phase orthorhombic olivine (Pnma) for all compositions, indicating that CuO addition up to 3 wt.% does not disrupt the parent lattice. Williamson–Hall analysis revealed a gradual reduction in crystallite size and micro strain with increasing CuO concentration, suggesting that the surface coating effectively suppresses grain growth and alleviates internal lattice distortions during calcination. Fourier-transform infrared spectroscopy preserved the characteristic $PO_4$ vibrational modes, verifying the integrity of the phosphate framework. Field-emission scanning electron microscopy combined with energy-dispersive X-ray mapping demonstrated a uniform distribution of Cu on particle surfaces, supporting the formation of a thin and homogeneous oxide layer. These combined results indicate that CuO acts as a structural stabiliser, promoting finer crystallites and enhanced lattice uniformity without generating secondary phases. Overall, this study provides clear experimental evidence that controlled CuO surface modification via PVA-assisted sol–gel synthesis can effectively tune the microstructure of $LiMnPO_4$ olivines. The findings enhance understanding of oxide–phosphate interactions and highlight the significance of surface engineering in achieving phase-pure, structurally stable olivine-type materials. Such insights can guide the design of compositionally optimised phosphate compounds for advanced functional and energy-related applications.

## Acknowledgement

The authors thank Universiti Teknikal Malaysia Melaka (UTeM) for its support of this work. We also wish to express our appreciation to Muhamad Akif Ibadillah Azwan for his assistance with the experimental work.

## Conflict of Interest

The authors declare that they have no conflict of interest regarding the publication of this paper.

## Author Contribution

*The authors are responsible for the study conception, research design, data collection, data analysis, result interpretation and manuscript drafting.*

## References


[1] Chen, Y., Kang, Y., Zhao, Y., et al. (2021) A review of lithium-ion battery safety concerns: The issues, strategies, and testing standards, Journal of Energy Chemistry, 59, 83–99. https://doi.org/10.1016/j.jechem.2020.10.017

[2] Mahmud, S., Rahman, M., Kamruzzaman, M., et al. (2022) Recent advances in lithium-ion battery materials for improved electrochemical performance: A review, Results in Engineering, 15, 100472. https://doi.org/10.1016/j.rineng.2022.100472

[3] Jyoti, J., Singh, B. P., & Tripathi, S. K. (2021) Recent advancements in development of different cathode materials for rechargeable lithium ion batteries, Journal of Energy Storage, 43, 103112. https://doi.org/10.1016/j.est.2021.103112

[4] Rui, X., Zhao, X., Lu, Z., et al. (2013) Olivine-type nanosheets for lithium ion battery cathodes, ACS Nano, 7, 5637–5646. https://doi.org/10.1021/nn4022263

[5] Yamada, A., Hosoya, M., Chung, S.-C., et al. (2003) Olivine-type cathodes: Achievements and problems, Journal of Power Sources, 119–121, 232–238. https://doi.org/10.1016/S0378-7753(03)00239-8

[6] Rajammal, K., Sivakumar, D., Duraisamy, N., et al. (2017) Influences of sintering temperatures and crystallite sizes on electrochemical properties of $LiNiPO_4$ as cathode materials via sol–gel route for lithium ion batteries, Journal of Sol-Gel Science and Technology, 83, 12–18. https://doi.org/10.1007/s10971-017-4372-5

[7] Wani, T. A., & Suresh, G. (2021) A comprehensive review of $LiMnPO_4$-based cathode materials for lithium-ion batteries: Current strategies to improve its performance, Journal of Energy Storage, 44, 103307. https://doi.org/10.1016/j.est.2021.103307

[8] Ragupathi, V., Panigrahi, P., & Nagarajan, G. S. (2019) Enhanced electrochemical performance of nanopyramid-like $LiMnPO_4$/C cathode for lithium–ion batteries, Applied Surface Science, 495, 143541. https://doi.org/10.1016/j.apsusc.2019.143541

[9] Sharmila, V., & Parthibavarman, M. (2021) Lithium manganese phosphate associated with MWCNT: Enhanced positive electrode for lithium hybrid batteries, Journal of Alloys and Compounds, 858, 157715. https://doi.org/10.1016/j.jallcom.2020.157715

[10] Rajammal, K., Ramesh, K., Ramesh, S., & Sivakumar, D. (2023) Doped olivine $LiMPO_4$ (M = Mn/Ni) derivatives as potential cathode materials for lithium-ion batteries: A mini review, Ionics, 29, 895–916. https://doi.org/10.1007/s11581-023-04894-3

[11] Wang, C., Li, S., Han, Y., & Lu, Z. (2017) Assembly of $LiMnPO_4$ nanoplates into microclusters as a high-performance cathode in lithium-ion batteries, ACS Applied Materials & Interfaces, 9, 27618–27624. https://doi.org/10.1021/acsami.7b05868

[12] Fu, X., Chang, K., Tang, H., et al. (2019) Environmentally compatible synthesis of $LiMnPO_4$/RGO using pure water system, Solid State Ionics, 337, 115–121. https://doi.org/10.1016/j.ssi.2019.04.018

[13] Zhu, C., Wu, Z., Xie, J., et al. (2018) Solvothermal-assisted morphology evolution of nanostructured $LiMnPO_4$ as high-performance lithium-ion battery cathode, Journal of Materials Science & Technology, 34, 1544–1549. https://doi.org/10.1016/j.jmst.2018.04.017

[14] Rajammal, K., Sivakumar, D., Duraisamy, N., et al. (2017) Na-doped $LiMnPO_4$ as an electrode material for enhanced lithium ion batteries, Bulletin of Materials Science, 40, 171–175. https://doi.org/10.1007/s12034-017-1365-5

[15] Rajammal, K., Sivakumar, D., Duraisamy, N., et al. (2016) Structural and electrochemical characterizations of $LiMn_{1-x}Al_{0.5x}Cu_{0.5x}PO_4$ (x = 0.0, 0.1, 0.2) cathode materials for lithium ion batteries, Materials Letters, 173, 131–135. https://doi.org/10.1016/j.matlet.2016.03.046

[16] Li, J., Liu, Z., & Ma, J. (2025) Preparation and improvement of electrochemical performance of Ni–Fe doped porous $LiMnPO_4$/C materials, Scientific Reports, 15, 1–11. https://doi.org/10.1038/s41598-025-12971-y

[17] Rajammal, K., Michalska, M., Ramesh, S., & D. S. (2025) Dual strategy of $Na^+$ doping and biomass-derived carbon coating from wheat starch carbon for high-performance $LiMnPO_4$ cathodes, Engineering Research Express. https://doi.org/10.1088/2631-8695/ae0de2

[18] Shobana, M. K. (2019) Metal oxide coated cathode materials for Li ion batteries – A review, Journal of Alloys and Compounds, 802, 477–487. https://doi.org/10.1016/j.jallcom.2019.06.194

[19] Rajammal, K., Sivakumar, D., Duraisamy, N., et al. (2016) Enhanced electrochemical properties of ZnO-coated $LiMnPO_4$ cathode materials for lithium ion batteries, Ionics, 22, 1551–1556. https://doi.org/10.1007/s11581-016-1685-2

[20] Rajammal, K., Arshid, N., & Sivakumar, D. (2024) Enhanced electrochemical properties of $Al_2O_3$-coated $LiNiPO_4$ cathode materials for lithium-ion batteries, Ionics, 30, 7929–7938. https://doi.org/10.1007/s11581-024-05894-7

[21] Gupta, K. K., Tan, C. P., Hsu, C. M., et al. (2023) Bio-polymer agar-assisted sol–gel synthesis and electrochemical characterization of bi-pyramidal $LiNi_{0.8}Co_{0.1}Mn_{0.1}O_2$ cathode materials for lithium-ion batteries, Journal of Sol-Gel Science and Technology, 108, 685–694. https://doi.org/10.1007/s10971-023-06212-9

[22] Li, B., Li, G., Zhang, D., et al. (2019) Unveiling the impact of the polypyrrole coating layer thickness on the electrochemical performances of $LiNi_{0.5}Co_{0.2}Mn_{0.3}O_2$ in Li–ion batteries, ChemistrySelect, 4, 6354–6360. https://doi.org/10.1002/slct.201901112

[23] Li, X., Shao, Z., Zhang, Y., et al. (2020) A facile polymeric gel route synthesis of high-voltage $LiNi_{0.5}Mn_{1.5}O_4$ cathode material for lithium-ion batteries, Materials Letters, 277, 128310. https://doi.org/10.1016/j.matlet.2020.128310

[24] Shi, M., Kong, L.-B., Liu, J.-B., et al. (2016) A novel carbon source coated on C-$LiFePO_4$ as a cathode material for lithium-ion batteries, Ionics, 22, 185–192. https://doi.org/10.1007/s11581-015-1549-1

[25] Jiang, T., Pan, W., Wang, J., et al. (2010) Carbon coated $Li_3V_2(PO_4)_3$ cathode material prepared by a PVA-assisted sol–gel method, Electrochimica Acta, 55, 3864–3869. https://doi.org/10.1016/j.electacta.2010.02.026

[26] Wang, J., Zhang, X., Liu, J., et al. (2010) Long-term cyclability and high-rate capability of $Li_3V_2(PO_4)_3$/C cathode material using PVA as carbon source, Electrochimica Acta, 55, 6879–6884. https://doi.org/10.1016/j.electacta.2010.05.077

[27] Sun, J., Li, Z., Ren, X., et al. (2019) High volumetric energy density of $LiFePO_4$/C microspheres based on xylitol-polyvinyl alcohol complex carbon sources, Journal of Alloys and Compounds, 773, 788–795. https://doi.org/10.1016/j.jallcom.2018.09.215

[28] Rajammal, K., Sivakumar, D., Duraisamy, N., et al. (2016) Effect of sintering temperature on structural properties of $LiMnPO_4$ cathode materials obtained by sol–gel method, Journal of Sol-Gel Science and Technology, 80, 514–522. https://doi.org/10.1007/s10971-016-4111-3

[29] Cao, Y., Xu, L., Xie, X., et al. (2019) Controllable synthesis of micro/nano-structured $LiMnPO_4$/C cathode with hierarchical spindle for lithium-ion batteries, Ceramics International, 45, 4886–4893. https://doi.org/10.1016/j.ceramint.2018.11.186

[30] Wu, Z., Long, Y. F., Lv, X. Y., et al. (2017) Microwave heating synthesis of spindle-like $LiMnPO_4$/C in a deep eutectic solvent, Ceramics International, 43, 6089–6095. https://doi.org/10.1016/j.ceramint.2017.02.001

[31] Hou, Y., Xu, Y., Jiang, S., et al. (2025) Precursor-driven carbon layer construction enables high-performance $LiMn_{0.5}Fe_{0.5}PO_4$ cathodes, Electrochimica Acta, 533, 146433. https://doi.org/10.1016/j.electacta.2025.146433

[32] El-Khalfaouy, R., Turan, S., Rodriguez, M. A., et al. (2021) A scalable approach for synthesizing olivine-structured $LiMn_{1-x}Co_xPO_4$/C high-voltage cathodes, Journal of Applied Electrochemistry, 51, 681–689. https://doi.org/10.1007/s10800-020-01528-8

[33] Kwon, S. N., Song, J., & Mumm, D. R. (2011) Effects of cathode fabrication conditions and cycling on the electrochemical performance of $LiNiO_2$ synthesized by combustion and calcination, Ceramics International, 37, 1543–1548. https://doi.org/10.1016/j.ceramint.2011.01.028

[34] Sathiyaraj, K., Gangulibabu, Bhuvaneswari, D., & Kalaiselvi, N. (2011) Effect of reaction temperature on morphology and electrochemical behavior: A comparative study on hydrothermal and co-precipitation synthesis of $LiCoO_2$ and $LiMn_2O_4$ using same set of precursors, Ionics, 17, 49–59. https://doi.org/10.1007/s11581-010-0482-6

[35] Kan, W. H., Deng, B., Xu, Y., et al. (2018) Understanding the effect of local short-range ordering on lithium diffusion in $Li_{1.3}Nb_{0.3}Mn_{0.4}O_2$ single-crystal cathode, Chem, 4, 2108–2123. https://doi.org/10.1016/j.chempr.2018.05.008

[36] Kumar, S., Chand, P., Kumar, A., & Anand, H. (2021) Effect of different aqueous electrolytes on electrochemical behavior of $LiFePO_4$ as a cathode material: Lithium ion battery and renewable energy nexus, Energy Nexus, 1, 100005. https://doi.org/10.1016/j.nexus.2021.100005

[37] Zhou, F., Zhu, P., Fu, X., et al. (2014) Comparative study of $LiMnPO_4$ cathode materials synthesized by solvothermal methods using different manganese salts, CrystEngComm, 16, 766–774. https://doi.org/10.1039/C3CE41567H